Comparison between Catalase-Peroxidase and Cytochrome *c* Peroxidase. The Role of the Hydrogen-Bond Networks for Protein Stability and Catalysis†

Elisa Santoni,‡ Christa Jakopitsch,§ Christian Obinger,§ and Giulietta Smulevich*,‡

Dipartimento di Chimica, Universitá di Firenze, Via della Lastruccia 3, I-50019 Sesto Fiorentino (FI), Italy, and Institute of Chemistry, BOKU - University of Natural Resources and Applied Life Sciences, Muthgasse 18, A-1190 Vienna, Austria

Received October 10, 2003; Revised Manuscript Received March 11, 2004

ABSTRACT: A detailed resonance Raman and electronic absorption investigation has been carried out on a series of novel distal and proximal variants of recombinant catalase-peroxidase from the cyanobacterium *Synechocystis* PCC 6803. In particular, variants of the distal triad Pro−Asp−Asn and the proximal triad His−Asp−Trp have been studied in their ferric and ferrous states at various pH. The data suggest marked differences in the structural role of the conserved residues and hydrogen-bond networks in KatG and CCP, which might be connected to the different catalytic activity. In particular, in KatG the proximal residues have a major role in the stability of the protein architecture because the disruption of the proximal Trp−Asp hydrogen bond by mutation weakens heme binding to the protein. On the distal side, replacing the hydrogen-acceptor carboxamide group of Asn153 by an aspartate carboxylate group or an aliphatic residue alters or disrupts the hydrogen bond with the distal His. As a consequence, the basicity of His123 is altered. The effect of mutation on Asp152 is noteworthy. Replacement of the Asp152 with Ser makes the architecture of the protein very similar to that of CCP. The Asp152 residue, which has been shown to be important in the hydrogen peroxide oxidation reaction, is expected to be hydrogen bonded to the nitrogen atom of Ile248 which is part of the KatG-specific insertion LL1, as in other KatGs. This insertion is at one edge of the heme, and connects the distal side with the proximal helices E and F, the latter carrying the proximal His ligand. We found that the distal Asp−Ile hydrogen bond is important for the stability of the heme architecture and its alteration changes markedly the proximal His−Asp hydrogen-bond interaction.

Catalase-peroxidases (KatGs)[1] are present in prokaryotes and fungi. They have a predominant catalase activity together with a substantial peroxidatic activity with broad specificity. On the basis of sequence similarity (*1*) KatGs have been recognized as part of class I of the peroxidase superfamily I (enzymes from plants, fungi, and bacteria). Moreover, recently the 2.0 Å crystal structure of KatG from the archaebacterium *Haloarcula marismortui* (*2*) and the 1.7 Å crystal structure of KatG from *Burkholderia pseudomallei* (*3*) revealed that the heme pocket contains catalytic residues virtually identical to the peroxidases belonging to class I peroxidases, such as cytochrome *c* peroxidase (CCP) and ascorbate peroxidase (APX). In particular, the distal and the proximal heme pocket contains the amino acid triad His, Arg, Trp, and His, Trp, Asp, respectively (Figure 1). However, in the vicinity of the active site of KatG novel covalent bonds are formed among the side chains of three residues including the conserved distal Trp, which seem to anchor a KatG-specific loop to the molecular surface and the substrate channel access (*2*, *4*, *5*). Moreover, inspection of the active site of KatG from *Haloarcula marismortui* shows an Asp residue as part of the substrate channel at the distal heme cavity. Its side chain carboxyl group pointing toward the heme pocket is 7.8 Å from the heme iron and hydrogen bonded to two water molecules, one being 5.9 Å from the iron atom, which are part of the extended hydrogen-bond network in the distal cavity of the heme pocket (Figure 1). The Asp is part of the triad Pro, Asp, Asn, the latter being hydrogen bonded to the distal His. This novel Asp residue, conserved in all KatGs, is not present in CCP or in APX. In particular, a Ser and an Ala residue replace the Asp residue of KatG in CCP and APX, respectively.

We have shown recently that mutation of the distal residues His, Arg, or Trp in the recombinant catalase-peroxidase from the cyanobacterium *Synechocystis* PCC 6803 not only affects selectively the functional activity of the protein (*6*, *7*), but in common with class I peroxidases alters the heme Fe coordination state and perturbs the proximal

† This work was supported by grants from the Ministry of Education, Universities, and Research (MIUR) to G.S., and by the Austrian Science Funds FWF (Project P15417) to C.O. and C.J. The authors acknowledge the COST action D21 "Metallo Enzymes and Chemical Biomimetics" for supporting the exchange among the different laboratories.

* To whom correspondence should be addressed. Tel: +39 055 4573083; fax: +39 055 457 3077; e-mail: giulietta.smulevich@unifi.it.

‡ Universitá di Firenze.

§ BOKU - University of Natural Resources and Applied Life Sciences.

[1] Abbreviations: KatG, catalase-peroxidase; CCP, cytochrome *c* peroxidase; CCP(MI), cytochrome *c* peroxidase expressed in *E. coli* containing Met−Lys−Thr at the N-terminus; APX, ascorbate peroxidase; HRPC, horseradish peroxidase isoenzyme C; WT, wild type; P151A, Pro151 → Ala; D152N, Asp152 → Asn; D152S, Asp152 → Ser; D152W, Asp152 → Trp; N153A, Asn153 → Ala; N153D, Asn153 → Asp; W341F, Trp341 → Phe; W341A, Trp341 → Ala; D402E, Asp402 → Glu; D402N, Asp402 → Asn; H290Q, His290 → Gln; CT1, long wavelength (>600 nm) porphyrin-to-metal charge-transfer band; RR, resonance Raman; 5-c, five coordinate; 6-c, six-coordinate; HS, high-spin; LS, low-spin.

10.1021/bi035835b CCC: $27.50
Published on Web 04/17/2004

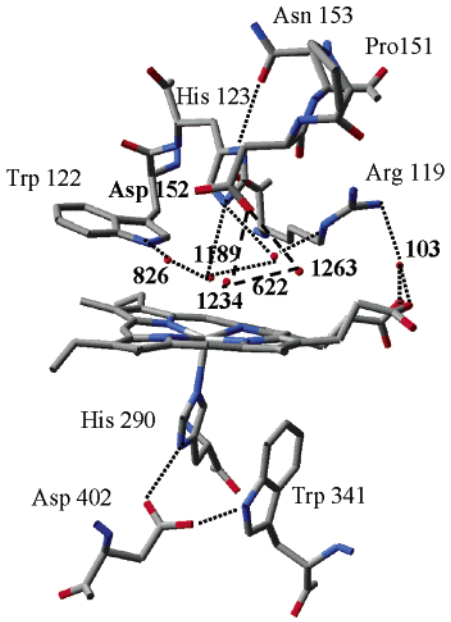

FIGURE 1: Structural diagram of the heme pocket of KatG according to the crystal structure of KatG from *Haloarcula marismortui* (*2*). (- - -), hydrogen-bonds inferred on the basis of distance criteria. Six observed distal water molecules are also shown.

Fe−Im bond strength. Moreover, it was shown that mutation alters the stability of the heme architecture, and in contrast to CCP or other plant peroxidases such as horseradish peroxidase (HRPC), the protein easily lost the heme prosthetic group when a negatively charged residue was placed in the distal cavity, as in the case of the H123E mutant (*8*). On the basis of the recently resolved X-ray structures, this instability could result from the repulsive effect induced by the vicinity of the negative charge of the carboxylate group of Asp152 residue which is present only in KatGs.

Therefore, in the present work we have extended the study to a series of novel mutants of the triad Pro, Asn, Asp on the distal side of the heme pocket (namely, P151A, D152N, D152S, D152W, N153A, and N153D) and present a comprehensive spectroscopic analysis that demonstrates the role of these residues in maintaining the stability of KatG. Moreover, a detailed spectroscopic study of the effect of mutation of the proximal triad His, Asp, Trp (namely, W341F and W341A, D402E and D402N, H290Q) has been carried out to establish possible interactions between the distal and proximal sides of the heme.

The mutation affects to different extents the coordination and spin states of the native protein. The changes are explained in terms of pH-dependent changes, charge location, size, and hydrogen-bonding acceptor/donor properties of the replacing amino acid. The data are compared with those of corresponding CCP variants (where available) and discussed in terms of the functional activity of the mutated proteins studied in parallel works (*9*−*11*).

MATERIALS AND METHODS

Mutagenesis, expression, and purification of KatG from *Synechocystis* PCC 6803 have been described previously (*6*, *9*, *10*).

The following buffers were used: 100 mM sodium phosphate at pH 7.0, 100 mM KH_2PO_4/100 mM citric acid at pH 6.5, 100 mM TRIS HCl at pH 8.0 and 8.5. The fluoride complexes were prepared by diluting concentrated protein in 500 mM NaF buffered with 500 mM sodium citrate at pH 6.4. The ferrous enzyme was obtained by adding a small volume (2−5 μL) of fresh sodium dithionite solution (20 g/L $Na_2S_2O_4 \cdot 2H_2O$) to a deoxygenated protein solution.

Sample concentration was about 0.03−0.06 mM for RR spectroscopy and about 0.05−0.1 mM for UV−visible absorption. The RR spectra were obtained by excitation with the 406.7 nm lines of a Kr^+ laser (Coherent, Innova 302) and with the 441.6 nm line of a He−Cd laser (Kimmon IK4121R−G). The backscattered light from a slowly rotating NMR tube was collected and focused into a computer-controlled double monochromator (Jobin-Yvon HG 2S) equipped with a cooled photomultiplier (RCA C31034A) and photon counting electronics. The RR spectra were calibrated with indene and CCl_4 as standards to an accuracy of ± 1 cm^{-1} for isolated bands. In the figures, the relative intensities of the high-frequency RR bands are normalized on the ν_4 band (not shown in the figures). To minimize local heating of the protein induced by the laser beam, the sample was cooled to approximately 15 °C by a gentle flow of N_2 gas passed through liquid N_2.

Peak intensities and positions of the bands in the 180−300 cm^{-1} frequency region of the RR spectra of ferrous KatGs and mutants were determined by a curve-fitting program (Tables 1 and 3).

Electronic absorption spectra were recorded at room temperature (23±1 °C) with a Cary 5 spectrophotometer, both prior to and after RR measurements to check if sample degradation had occurred under the experimental conditions.

RESULTS

Mutation of the Proximal Triad His−Asp−Trp. We have studied the resonance Raman (RR) and electronic absorption spectra of the following mutants of KatG obtained by site-specific mutagenesis: Asp402 → Asn, Glu (D402N, D402E) in which the Asp carboxylate group, which acts as hydrogen-bond acceptor to the proximal His290 ligand of the heme Fe, is replaced by either a carboxamide group of an Asn or a carboxylate group of a Glu residue; Trp341 → Phe, Ala (W341F, W341A) in which the proximal Trp hydrogen bonded to Asp402 is replaced by the non-hydrogen-bonding aromatic residue Phe or aliphatic residue Ala; His290 → Gln(H290Q) in which the proximal Fe atom ligand has been converted to the polar Gln residue.

Ferric Form. At neutral pH the UV−Vis spectrum of native KatG, with a Soret band at 407 nm, Q-bands at 502 and 542 nm and a CT1 band at 637 nm, is indicative of a five-coordinate (5-c) high-spin (HS) heme coexisting with an aquo six-coordinate (6-c) HS heme (*8*). As previously reported (*9*), only the W341F variant retains spectral features similar to the wild type (WT) protein, giving rise to a spectrum characteristic of a mixture of HS hemes (data not shown). However, the blue-shift of the CT1 band to 628 nm suggests the presence of a higher amount of an aquo 6-c HS species as compared to the WT protein. Moreover, weak bands in the 570−590 nm region indicate the presence of a 6-c low-spin (LS) heme as previously reported for the corresponding W321F mutant of *Mycobacterium tuberculosis* KatG (*12*). All the other variants give rise to spectra that are typical of a 6-c LS heme, with Soret band in the range

Table 1: Spectral Parameters of the RR Bands of the Ferrous Forms of the WT KatG and the Various Mutants at pH 6.5 in the 200−300 cm^{-1} Region Obtained by a Band-Fitting Program Using Lorentzian Line Shapes[a]

		ν (Fe−Im)[b]	ν (Fe−Im)			ν (Fe−Im)	ν (Fe−Im)		
KatG WT	ν (cm^{-1})	**202**		226	233		**251**	267	284
	$\Delta\bar{\nu}$(cm^{-1})	16		17	19		19	19	16
	I (%)	21		5	17		36	13	8
W341F	ν (cm^{-1})	***205***		226	233		***253***	267	284
	$\Delta\bar{\nu}$ (cm^{-1})	15		17	19		19	19	21
	I (%)	18		1	12		33	22	14
D402E	ν (cm^{-1})	**202**	**213**	226	233	**239**	**251**	265	284
	$\Delta\bar{\nu}$ (cm^{-1})	19	19	17	19	19	19	19	16
	I (%)	13	4	2	5	25	31	15	5
D152N	ν (cm^{-1})	***204***		226	233		**251**	267	284
	$\Delta\bar{\nu}$ (cm^{-1})	19		17	19		19	19	19
	I (%)	21		6	17		36	12	8
D152S	ν (cm^{-1})	***204***		226	hidden	***237***	***250***	267	284
	$\Delta\bar{\nu}$ (cm^{-1})	17		17		19	19	19	12
	I (%)	25		8		20	34	9	4
D152W	ν (cm^{-1})	***205***		226	hidden	***237***	***254***	270	284
	$\Delta\bar{\nu}$ (cm^{-1})	19		17		19	19	19	19
	I (%)	15		10		12	43	11	9
N153A	ν (cm^{-1})	***201***		226	233	***237***	**251**	267	284
	$\Delta\bar{\nu}$ (cm^{-1})	19		17	19	19	19	19	19
	I (%)	31		10	4	20	24	6	5
N153D	ν (cm^{-1})	***204***		226	233		**251**	271	284
	$\Delta\bar{\nu}$ (cm^{-1})	19		17	19		19	19	19
	I (%)	22		2	18		43	10	5
P151A	ν (cm^{-1})	***204***		226	233		***252***	270	284
	$\Delta\bar{\nu}$ (cm^{-1})	19		17	19		19	19	19
	I (%)	21		8	15		38	12	6

[a] Frequencies (ν) and bandwidths ($\Delta\bar{\nu}$) are given in cm^{-1}. The band intensities (I) are in arbitrary units expressed as %. [b] In bold are indicated the ν (Fe−Im) stretching mode frequency of wild-type KatG; in bold and italics are the frequencies of the bands which are changed as compared to WT; the new ν (Fe−Im) stretching mode not observed in wild-type KatG is underlined.

Table 2: Apparent K_m and k_{Cat} Values for the Catalase Activity of Wild-Type and Variants of Catalase-Peroxidase from *Synechocystis* PCC 6803[a]

	catalase activity		peroxidase activity
	K_m (mM)	k_{cat} (s^{-1})	*o*-dianisidine (units mg^{-1})
KatG	(4.1 ± 0.2)	(3500 ± 350)	(3.2 ± 0.3)
D152N	(2.5 ± 0.1)	(95 ± 9)	(7.5 ± 0.4)
D152S	(2.4 ± 0.2)	(200 ± 25)	(7.6 ± 0.4)
D152W	(3.2 ± 0.3)	(20 ± 4)	(21.5 ± 0.1)
P151A	(2.5 ± 0.1)	(2500 ± 190)	(2.4 ± 0.2)
W341F	(6.3 ± 0.2)	(1460 ± 150)	(6.1 ± 0.4)
W341A	(4.3 ± 0.1)	(16 ± 4)	(0.8 ± 0.1)
H290Q	(15 ± 0.1)	(3 ± 1)	(0.18 ± 0.05)
D402N	(6.4 ± 0.3)	(17 ± 4)	(1.8 ± 0.2)
D402E	(5.9 ± 0.2)	(21 ± 4)	(2.1 ± 0.2)

[a] Also given are specific peroxidase activities (units per mg protein). Reaction conditions: 50 mM phosphate buffer, pH 7 and 30 °C (*9*−*11*).

412−418 nm, and Q-bands at about 570−590 nm. In addition, a shoulder at 368 nm, which increases in the order D402E, D402N, W341A, and H290Q, indicates the presence of free heme (data not shown). Accordingly, the Reinheitszahl decreases in the same order (KatG, 0.57; W341F, 0.6; D402E, 0.35; D402N, 0.33; W341A, 0.22; H290Q, 0.2) as previously reported (*9*). Figure 2 compares the RR spectra of WT KatG with the W341F and D402E variants. While the latter gives rise to a typical 6-c LS spectrum (ν_3 at 1505 cm^{-1}, ν_2 at 1582 cm^{-1}, and ν_{10} at 1639 cm^{-1}) the W341F variant shows an increased amount of the 6-c HS (ν_3 at 1484 cm^{-1}, ν_2 at 1566 cm^{-1}) coexisting with the 5-c HS form (ν_3 at 1495 cm^{-1}, ν_2 at 1573 cm^{-1}, and ν_{10} at 1631 cm^{-1}) compared to WT. The RR spectra of the other variants are very similar to that of D402E, characterized by core size marker bands of a LS heme and 5-c HS, due to the free heme (data not shown). Interestingly, in the spectrum of the D402E variant the vinyl stretches give rise to two strong bands at 1623 and 1634 cm^{-1}, compared to the corresponding bands of WT KatG at 1624 cm^{-1} (weak) and 1629 cm^{-1} (strong) (*8*). Similar spectral features are also observed for the D402N and W341A mutants. A direct relationship between the ν(C═C) vinyl stretching frequency and the orientations of the vinyl groups, as induced by specific protein interaction, was established recently for the superfamily of plant peroxidases (*13*). In particular, it was found that, when the protein matrix exerts no constraints on the vinyl groups, two distinct ν(C═C) stretching modes are observed in the RR spectrum as found in model compounds in solution (*14*). Therefore, an increase in frequency is consistent with further reduced steric constraints in the near proximity of the vinyl bond, resulting from a major architecture readjustment.

Upon addition of NaF at pH 6.4, only the W341F variant bound fluoride completely, giving rise to a spectrum very similar to that of the WT KatG-F complex (data not shown) (*8*), while the internal ligand bound to the heme iron giving rise to the LS heme in the D402E mutant could not be displaced by the fluoride.

Ferrous Form. The structural changes observed in the ferric forms are conserved upon reduction. At pH 6.5, the UV−Vis spectra of the reduced proteins indicate that only the W341F variant gives rise to a spectrum similar to the WT protein, with the Soret band at 438 nm and Q-bands at 557 and 581 nm (data not shown). The spectrum corresponds to a 5-c HS species. However, in common with the WT protein, the variant shows also a shoulder at 420 nm due to the presence of a 6-c LS form probably due to the binding

Table 3: Spectral Parameters of the RR Bands of the Ferrous Forms of KatG and the D152S and D152W Mutants in the 200−300 cm^{-1} Region at Different pH Obtained by a Band-Fitting Program Using Lorentzian Line Shapes[a]

		ν (Fe−Im)[b]			ν (Fe−Im)	ν (Fe−Im)		
KatG pH 6.5	ν (cm^{-1})	**202**	226	233		**251**	267	284
	$\Delta\bar{\nu}$ (cm^{-1})	16	17	19		19	19	16
	I (%)	21	5	17		36	13	8
KatG pH 5.7	ν (cm^{-1})	***205***	226	236		***253***	269	284
	$\Delta\bar{\nu}$ (cm^{-1})	17	17	19		19	19	19
	I (%)	20	8	15		36	12	9
D152S pH 6.5	ν (cm^{-1})	***204***	226	hidden	**237**	***250***	267	284
	$\Delta\bar{\nu}$ (cm^{-1})	17	17		19	19	19	12
	I (%)	25	8		20	34	9	4
D152S pH 8.0	ν (cm^{-1})	***202***	226	hidden	**237**	***250***	269	284
	$\Delta\bar{\nu}$ (cm^{-1})	19	17		19	19	19	12
	I (%)	32	7		24	24	10	3
D152W pH 6.5	ν (cm^{-1})	***205***	226	hidden	**237**	***254***	270	284
	$\Delta\bar{\nu}$ (cm^{-1})	19	17		19	19	19	19
	I (%)	15	10		12	43	11	9
D152W pH 8.5	ν (cm^{-1})	***203***	226	hidden	**237**	***252***	269	284
	$\Delta\bar{\nu}$ (cm^{-1})	19	17		19	19	19	19
	I (%)	18	12		17	35	13	5

[a] Frequencies (ν) and bandwidths ($\Delta\bar{\nu}$) are given in cm^{-1}. The band intensities (*I*) are in arbitrary units expressed as %. [b] In bold are indicated the ν (Fe−Im) stretching mode frequency of wild-type KatG; in bold and italics are the frequencies of the bands which are changed as compared to WT; the new ν (Fe−Im) stretching mode not observed in wild-type KatG is underlined.

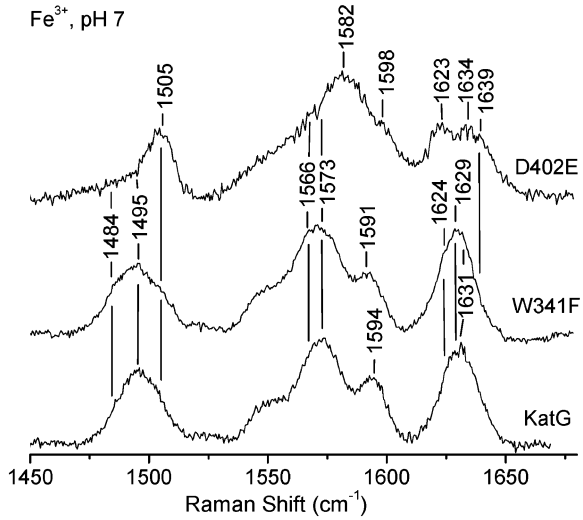

FIGURE 2: RR spectra in the high-frequency region of ferric KatG and proximal mutants W341F and D402E at pH 7.0 obtained with 406.7 nm excitation wavelength. Experimental conditions: 5 cm^{-1} resolution; (KatG) 16 s/0.5 cm^{-1} collection interval and 15 mW laser power at the sample; (W341F) 45 s/0.5 cm^{-1} collection interval and 10 mW laser power at the sample; (D402E) 38 s/0.5 cm^{-1} collection interval and 10 mW laser power at the sample.

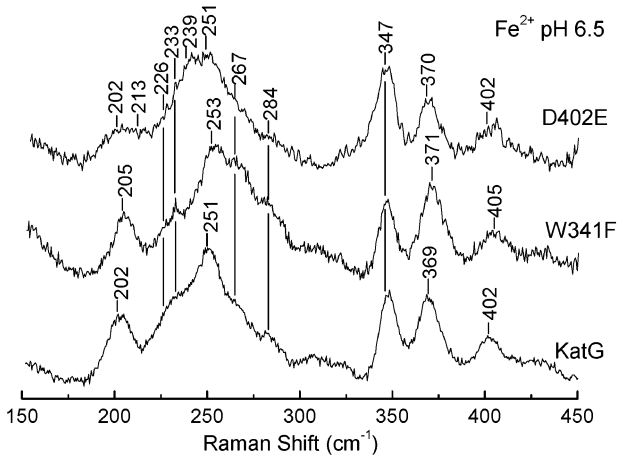

FIGURE 3: RR spectra in the low-frequency region of ferrous KatG and proximal mutants W341F and D402E at pH 6.5 obtained with 441.6 nm excitation wavelength. Experimental conditions: 5 cm^{-1} resolution; (KatG) 30 s/0.5 cm^{-1} collection interval and 20 mW laser power at the sample; (W341F) 35 s/0.5 cm^{-1} collection interval and 25 mW laser power at the sample; (D402E) 65 s/0.5 cm^{-1} collection interval and 25 mW laser power at the sample.

of an internal ligand. In the D402E variant, the 6-c LS form increases at the expense of the HS form; the LS species becomes dominant in all the other variants. As previously found for other KatG mutants (*8*), the 6-c LS form appears to be connected to the loss of the heme prosthetic group. The amount of LS, in fact, is very high in the W341A and H290Q variants, which show also a high amount of free heme as indicated by a band at 385 nm.

Upon excitation with the 441.6 nm line, the 5-c HS ferrous heme is mainly enhanced in the RR spectrum. Therefore, the low-frequency region gives information on the Fe−Im bond strength via the frequency of the Fe−Im stretching mode, which is active only in the ferrous 5-c species. In peroxidases, the hydrogen bond between the N_δ atom of the imidazole fifth ligand and the oxygen atom of the Asp carboxylate group gives the proximal ligand imidazolate character and results in both a strengthening of the Fe−Im bond and a higher frequency of the associated vibrational mode, as compared to other heme proteins. Therefore, due to its sensitivity to the Fe−Im bond strength, the ν(Fe−Im) stretching mode is a useful probe of either the hydrogen-bond strength between the conserved proximal His (His290) and the Asp residue (Asp402), or the hydrogen bond between the Asp residue (Asp402) and the nitrogen atom of the indole group of the Trp341.

Figure 3 compares the low-frequency RR spectra of the WT protein with the W341F and D402E variants. No information could be obtained for the other variants because they are all 6-c LS heme. At pH 6.5, two independent ν(Fe−Im) stretching modes were found in the WT enzyme at 251 and 202 cm^{-1} (*8*). In the W341F variant, these bands upshift by 2−3 cm^{-1}, indicating that the disruption of the hydrogen bond between the W341 and the D402 has strengthened the Fe−Im bond. Moreover, the band at 267 cm^{-1} increases in

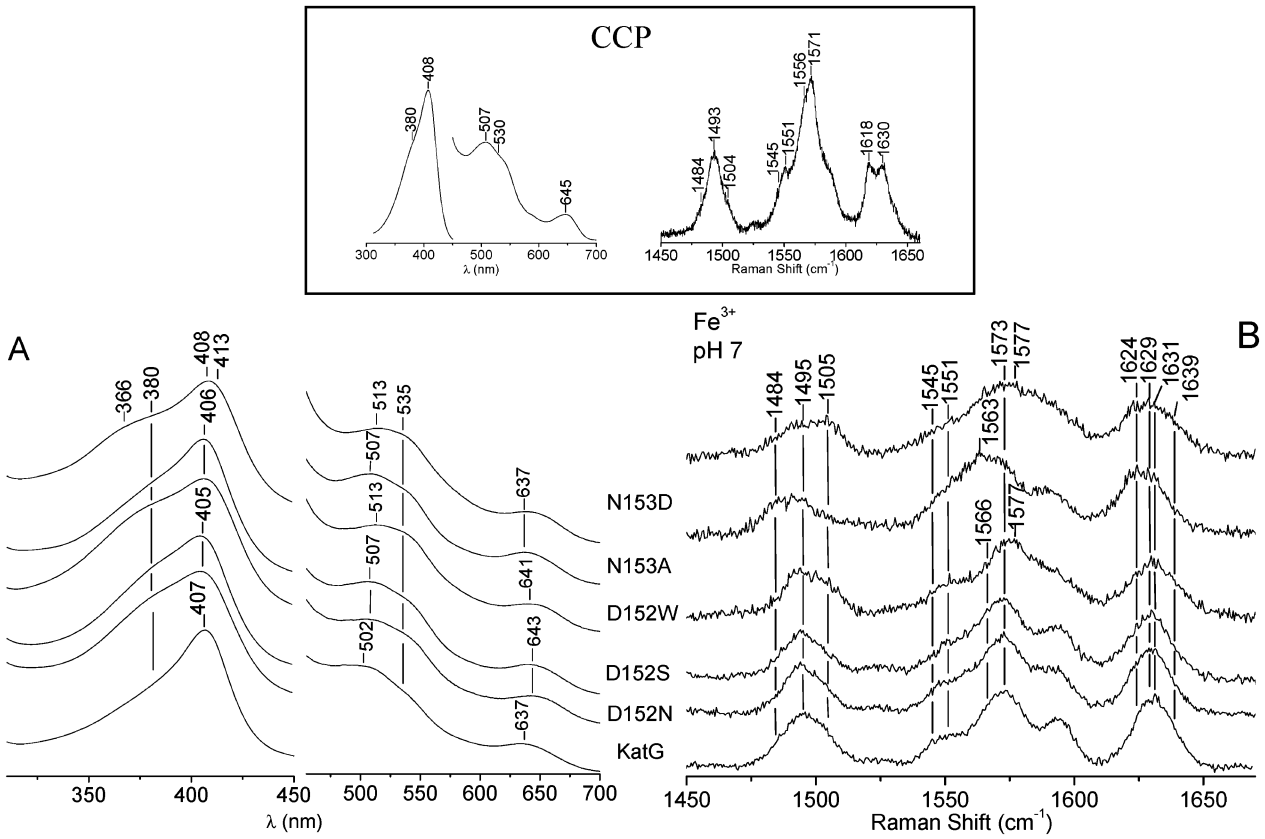

FIGURE 4: Electronic absorption (A) and RR (B) spectra of ferric KatG and the distal mutants D152N, D152N, D152S, D152W, N153A, and N153D at pH 7.0. (A) The region between 490 and 700 nm has been expanded 5-fold. (B) The RR spectra have been obtained with 441.6 nm excitation wavelength. Experimental conditions: 5 cm^{-1} resolution, 15 mW laser power at the sample; (KatG) 16 s/0.5 cm^{-1} collection interval; (D152N) 24 s/0.5 cm^{-1} collection interval; (D152S) 19 s/0.5 cm^{-1} collection interval; (D152W) 9 s/0.5 cm^{-1} collection interval; (N153A) 6 s/0.5 cm^{-1} collection interval; (N153D) 7 s/0.5 cm^{-1} collection interval. The inset shows the electronic absorption (the region between 490 and 700 nm has been expanded 6-fold) and RR spectra (413.1 nm excitation wavelength, 30 mW laser power at the sample, 5 cm^{-1} resolution, 5 s/0.5 cm^{-1} collection interval) of ferric CCP(MI) at pH 7.0.

intensity. This latter band is assigned to an internal mode of the His ligand whose RR enhancement is attributed to vibrational coupling with the nearby Fe−His modes (*15*).

The spectrum of the D402E variant appears of particular interest, since new bands are clearly detected. Deconvolution of the spectra by curve-fitting (Table 1) revealed the presence of new bands at 213 and 239 cm^{-1}, which grow at the expense of the bands at 202 and 251 cm^{-1}. The D402E spectrum is, therefore, consistent with the presence of two different conformers each characterized by two Fe−Im stretching modes, at 202 and 251 cm^{-1}, as the WT enzyme, and at 213 and 237 cm^{-1}.

Mutation of the Distal Triad Pro-Asp-Asn. We have studied the RR and electronic absorption spectra of the following KatG variants obtained by site-specific mutagenesis: Pro151 → Ala (P151A), in which the cyclic five membered ring of Pro is replaced by the aliphatic residue Ala; Asp152 → Trp and Asn (D152W, D152N) in which the Asp carboxylate group, which acts as hydrogen-acceptor with two distal water molecules, is replaced by a hydrogen-bond donor of either the indole group of a Trp residue or the carboxamide group of an Asn residue. Moreover, the Asp152 was replaced by a Ser residue (D152S) to mimic the triad Pro−Ser−Asn present in CCP. Finally, we investigated the mutations Asn153 → Asp and Ala (N153D, N153A) in which the conserved carboxamide group, which acts as a hydrogen acceptor with the distal His, is replaced by an Asp carboxylate group or an aliphatic residue Ala.

Ferric Form. The distal Pro residue is conserved in KatGs and in all plant peroxidases but is not involved in the catalytic mechanism. Therefore, its alteration might provide information on the impact of this distal mutation on the architecture of the heme pocket. The similarity of the electronic and RR spectra of the P151A mutant with those of the WT protein (data not shown) indicates that this mutation does not alter the heme pocket, in agreement with previous results showing that this mutation had only minor effects on the bifunctional activity of the enzyme (Table 2) (*11*).

The effect of mutation on Asp152 is noteworthy. While the D152N and D152S variants were very stable, the shoulder at about 368 nm in the D152W mutant indicates the presence of some free heme. The spectra of the three variants, however, with an intense shoulder at 380 nm and the red-shift of the CT1 band to 643 nm (D152N and D152S) and 641 nm (D152W) (Figure 4 A) indicate that the mutation of the aspartic residue increases the 5-c HS form at the expense of the aquo 6c species. In particular, the spectra of D152N and D152S are very similar to CCP (*16*, *17*). The RR spectra confirm these conclusions (Figure 4 B). The D152N and D152S mutants are mainly 5-c HS species (ν_3 at 1495 cm^{-1}, ν_2 at 1573 cm^{-1}, and ν_{10} at 1631 cm^{-1}), giving rise to spectra that resemble very closely those of CCP (*16*, *17*). The D152W variant is characterized by the presence of free heme and a 6-c LS species. The bulky indole ring seems to destabilize the protein.

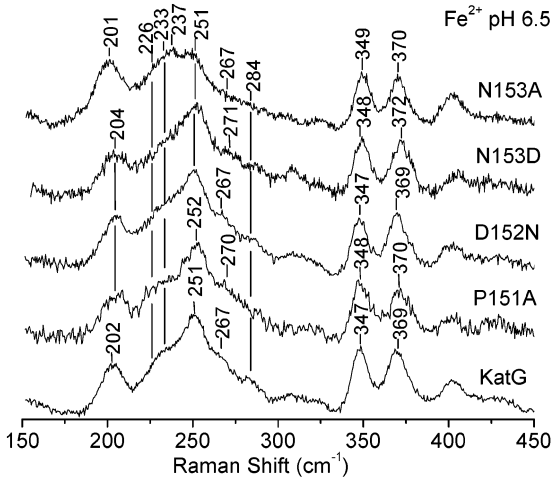

FIGURE 5: RR spectra in the low-frequency region of ferrous KatG and distal mutants P151A, D152N, N153D, and N153A at pH 6.5 obtained with 441.6 nm excitation wavelength. Experimental conditions: 5 cm^{-1} resolution, 20 mW (KatG) and 22 mW (distal mutants) laser power at the sample; (KatG) 30 s/0.5 cm^{-1} collection interval; (P151A) 6 s/0.5 cm^{-1} collection interval; (D152N) 14 s/0.5 cm^{-1} collection interval; (N153D) 11 s/0.5 cm^{-1} collection interval; (N153A) 18 s/0.5 cm^{-1} collection interval.

Exchange of the distal Asn153 with Ala or Asp has an opposite effect with respect that observed for the Asp152 mutation (Figure 4). Replacing the Asn residue by Ala causes an increase of the 6-c HS heme (ν_3 at 1484 cm^{-1}, ν_2 at 1563 cm^{-1}), whereas in the N153D variant an increase of 6-c LS heme is observed (ν_3 at 1505 cm^{-1}, ν_2 at 1587 cm^{-1}, and ν_{10} at 1639 cm^{-1}). In addition, the shoulder at 368 nm in the electronic absorption spectrum clearly indicates the presence of free heme. No change in the frequency of the vinyl stretching modes is observed for the variants of the Pro−Asp−Asn triad.

The binding of fluoride appears to be affected by mutation. Upon addition of fluoride to the variants an amount of unbound protein higher than that of the native protein was observed. The effect was markedly evident in the UV−Vis spectra of the N153A variant (data not shown).

Ferrous Form. No changes are observed in the UV−Vis spectra of the D152N, D152S, D152W, and N153A variants as compared to the WT KatG (data not shown). They are typical of mainly 5-c HS ferrous hemes, with bands at 439, 557, and 587 nm. On the contrary, unlike the ferric form which has very similar behavior compared to the WT protein, the ferrous form of the P151A mutant is clearly characterized by an increased amount of LS heme (shoulders at 423 and 531 nm). The same conclusion can be drawn for the N153D variant which shows also a band at 385 nm due to the presence of free heme. The corresponding RR spectra of these distal mutants in the high frequency region are also very similar, characteristic of a 5-c HS heme with an increased contribution of the 6-c LS heme for the P151A and N153D mutants (data not shown). In the low frequency region, no significant changes are observed in the spectra of the P151A, D152N, and N153D variants (Figure 5 and Table 1) (only a slight shift by 1−2 cm^{-1} is observed for the ν(Fe−Im) stretching mode at lower frequency), indicating that these distal mutations do not significantly affect the protein structure on the proximal side of the heme. On the contrary, the N153A, D152S, and D152W mutations significantly alter the frequency and/or the intensity of the ν(Fe−Im) stretching modes (Figures 5 and 6). In particular, visual inspection (Figure 5) and deconvolution of the spectrum by curve-fitting (Table 1) revealed that the N153A spectrum is characterized by the presence of a new band at 237 cm^{-1}, which is overlapped with the porphyrin mode at 233 cm^{-1}, and an increase in intensity of the band at 201 cm^{-1}. Since the hydrogen bond between the N_δ of the imidazole ligand of the proximal His290 and the oxygen atom of the Asp402 makes the frequency of the ν(Fe−Im) stretching mode pH-dependent, we tried to confirm the presence of a new Fe−Im stretch at 237 cm^{-1} by changing the pH of the solution. However, at pH 8.0 the variant was completely converted to LS and at pH 5.7 the protein was not stable and precipitated. At pH 6.5, the D152S variant shows also the presence of a new band at 237 cm^{-1} which increases in intensity at alkaline pH with a concomitant decrease of the intensity of the band at 250 cm^{-1}. Upon changing the pH, the band observed at 204 cm^{-1} shifts down by 2 cm^{-1} and also increases in intensity (Figure 6 and Table 3). A similar result is also obtained for the D152W variant: at pH 8.5 a

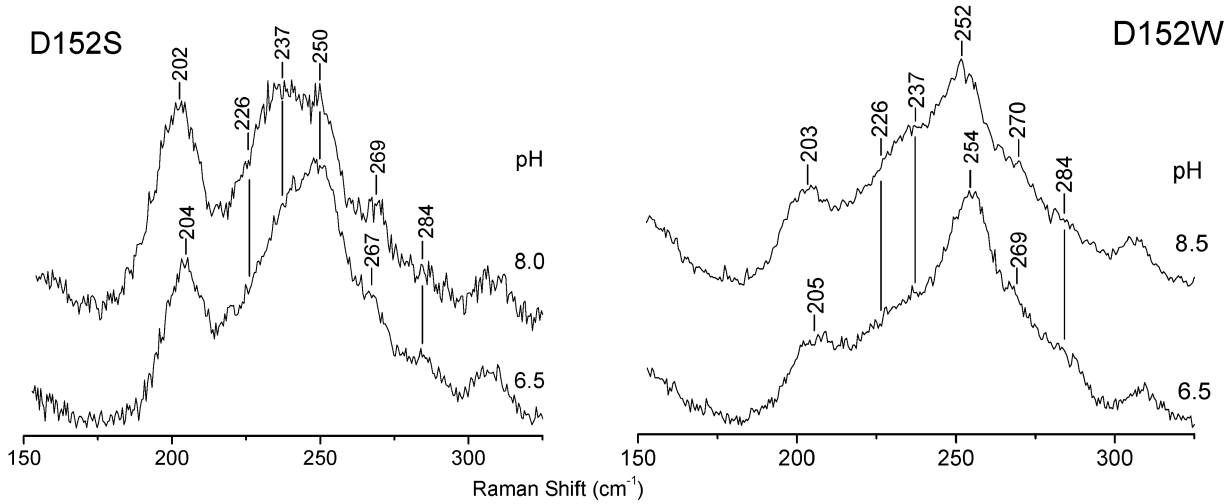

FIGURE 6: RR spectra in the low-frequency region (150−325 cm^{-1}) of ferrous distal mutants D152S and D152W obtained with 441.6 nm excitation wavelength. Experimental conditions: 5 cm^{-1} resolution; (D152S) at pH 6.5 21 s/0.5 cm^{-1} collection interval and 22 mW laser power at the sample; at pH 8.0 50 s/0.5 cm^{-1} collection interval, 20 mW laser power at the sample; (D152W) at pH 6.5 31 s/0.5 cm^{-1} collection interval 22 mW laser power at the sample; at pH 8.5 25 s/0.5 cm^{-1} collection interval 18 mW laser power at the sample.

new weak band is observed at 237 cm^{-1}. Moreover, both the ν(Fe−Im) stretching modes observed in the WT protein at 202 and 251 cm^{-1} are upshifted by 3 cm^{-1} at pH 6.5 and appear to be pH sensitive (Figure 6 and Table 3).

DISCUSSION

Mutation of the Proximal Triad His−Asp−Trp. Central to the peroxidase mechanism are the invariant distal side residues, His123 and Arg119 (KatG numbering), which work in concert to stabilize the charge separation required in the heterolytic fission of the peroxide O−O bond. Less clear is the precise role of the proximal ligand and the hydrogen-bond network involving the His, Asp, and Trp residues. In plant, fungal, and bacterial peroxidases as well as in KatG, a hydrogen bond between the N_δ atom of the proximal His and the oxygen atom of the Asp side chain gives the proximal ligand an imidazolate character; moreover, the other oxygen atom of the Asp side chain is hydrogen bonded with the N atom of the indole group of a Trp residue.

Site-directed mutagenesis on the proximal side of CCP showed that the function of the proximal residues may be regulation of the iron redox potential, stabilizing the ferryl intermediate of compound I, assisting in cleavage of the peroxide O−O bond, and/or simply helping to hold the heme in place (*16*, *18*, *19*). Unlike CCP, altering the proximal side of KatG dramatically alters its activity (*9*) and the stability of the heme architecture and weakens the heme binding. The present results give further evidence that mutation of the proximal residues alters the hydrogen-bond network connecting the proximal and the distal side of the heme pocket. These effects, however, depend not only on the type of residue that is mutated and/or the hydrogen bond that is altered, but also on the size and the charge of the residue replacing the native amino acid. The most dramatic effect is observed for the conversion of the proximal His ligand to Gln(H290Q). This mutation gives rise to an almost completely inactive protein (*9*) (Table 2), corresponding to an almost complete conversion to a LS heme which coexists with a high amount of free heme. Conversely, the corresponding mutation in CCP (H175Q) (*20*), which gives rise to a 6-c HS heme, does not affect the protein activity, and results in very little change in the structure outside of the immediate vicinity of the mutation.

Replacing the Trp side chain with the aliphatic Ala (W341A) in KatG resulted in the binding of an internal ligand to the iron atom on the distal side of the heme cavity giving rise to 6-c LS heme with the concomitant appearance of free heme. The mutation of the corresponding Trp residue (Trp191) in CCP by either aromatic amino acids (such as Phe or Tyr) or aliphatic residues (Gly or Gln) does not perturb protein stability. The crystal structures of the W191G or W191Q CCP variants revealed a monovalent cation binding site in the cavity formerly occupied by the side chain of Trp191 (*19*) which influences the affinity for hydroxide binding to the heme iron (unpublished results) and is accompanied by a significant conformational change in the loop containing Trp191. Thus, loss of the Trp191−Asp235 interaction in CCP allows the protein some flexibility. However, the extent of the mutation induced flexibility is greater in KatG where the Trp341−Asp402 interaction is lost. Only the W341F variant maintains almost all the spectroscopic and kinetic characteristics of the WT KatG. The overall catalase activity was slightly decreased, whereas the peroxidase activity was enhanced (Table 2) (*9*). This latter effect is in marked contrast with the results obtained for the corresponding CCP variant (W191F). It maintains the crystal structure, coordination, and spin states essentially unchanged compared to the WT protein (*16*, *21*), but is almost inactive (*22*). Since in CCP the proximal Trp is the site of the free radical formation in compound I (*23*), the Trp → Phe variant is inactive as the electron-transfer pathway from ferrocytochrome *c* is broken. On the contrary, in KatG the intermediate compound I has been assigned to an oxyferryl iron porphyrin π cation radical as for APX and all the other known peroxidases (*9*−*11*, *24*−*26*). Interestingly, the electrostatic environment in the vicinity of the proximal His, Asp, and Trp residues does not resemble that of APX, but it is similar to that of CCP (*2*). A potassium ion near the Trp at the proximal side of the heme in APX, considered essential for the formation of the porphyrin π cation radical, is replaced by a water molecule in both CCP and *Haloarcula marismortui* KatG (*2*). In addition, superimposition of the N-terminal segment of both *Haloarcula marismortui* (*2*) and *Burkholderia pseudomallei* (*3*) onto CCP revealed a great conservation of the structures. However, the disruption of the hydrogen bond between the N atom of the indole ring of the Trp residue and the carboxylate oxygen atom of the Asp residue in the KatG W341F variant strengthens the Fe−Im bond. This effect has been previously observed only in the corresponding W191G and W191Q CCP variants (unpublished results), where the cavity created by the missing Trp side chain is occupied by a cation (*19*). The effects were not observed for the W191F CCP variant (*16*). We attribute the strengthening of the Fe−Im stretches to the strengthening of the His−Asp interaction. This might derive from the reduction of steric constraints imposed on the proximal His residue by the hydrogen bond between the N atom of the indole ring of the Trp residue and the oxygen atom of the Asp residue, which is in turn hydrogen bonded to the N_δ atom of the imidazole of the His ligand. A similar result has been obtained for the corresponding F221M variant of HRPC (*27*). In that case, the reduction of the steric constraints imposed on the proximal His residue was interpreted as due to the loss of the $\pi \rightarrow \pi^*$ interaction between the aromatic rings of His170 and Phe221. Inspection of the structure of KatG from *Haloarcula marismortui* shows that the proximal His and Trp are stacked almost parallel in KatG. However, considering that replacing the aromatic ring of Trp by the small aliphatic Ala side chain strongly destabilizes the entire protein, the effect observed for the W341F variant is more likely due to disruption of the Trp−Asp hydrogen bond, whereas the combined effect of the disruption of the Trp−Asp hydrogen bond and alteration of the $\pi \rightarrow \pi^*$ interaction between the His and the aromatic ring in the W341A variant destabilizes the protein architecture.

A dramatic effect on the overall structure of KatG is also observed upon mutation of the proximal Asp402 residue. While the Asp−Asn mutation gave rise to an almost complete 6-c LS heme and an increased amount of the free heme, maintaining a carboxylate group in the proximal region with the Asp−Glu mutation partially preserved the hydrogen-bond interaction with the N_δ atom of the proximal His. As a consequence, the heme binding was only partially disrupted

and, therefore, the protein maintained its native HS character to some extent. Moreover, in the region of the Fe−Im stretches, in addition to the two Fe−Im stretches typical of the WT, two new ν(Fe−Im) stretching modes due to the replacement of the Asp−His hydrogen bond by the Glu−His hydrogen bond are observed. This result is in marked contrast with CCP (*18*). In fact, unlike the D402E KatG variant, the replacement of Asp235 with Glu, Asn, or Ala in CCP appears to result in a significantly weaker hydrogen bond in which the proton resides essentially on His175 [ν(Fe−Im) stretching mode at 205 cm^{-1}]. The X-ray structure showed that the replacement of Asp235 by Glu introduces only very little perturbation at the enzyme active site with only minor changes in the geometry of its carboxylate interactions with both Trp191 and His175. No changes were evident at the Trp191 free radical site. Therefore, the small changes in the hydrogen-bond geometry have apparently important effects increasing the reduction potential by 70 mV, altering the anisotropy of the Trp191 free radical EPR, affecting the activity and the spin-state equilibrium, and reducing the strength of the iron ligand field as measured by the zero-field splitting. The effect of exchanging of the proximal Asp 235 by Asn or Ala are even more dramatic causing alteration of the coordination state, redox potential (increased by 110 mV), electronic structure, and function of the enzyme. Therefore, the Asp-to-Glu mutation in CCP introduced very little perturbation in the structure, and the protein retained about 40% of the WT activity (*18*); the exchange of Asp by Asn altered markedly the electronic structure and the function of the protein (*16*). In the case of KatG, both D402E and D402N variants showed drastically reduced catalase activity, whereas the peroxidase activity was much less affected (Table 2) (*9*).

Mutation of the Distal Triad Pro−Asp−Asn. The spectral data of the ferric form indicate that mutation of these distal residues does not significantly alter the interaction between the heme and the protein. The only exception is represented by the N153D variant, which shows the presence of a significant amount of free heme in both its ferric and ferrous forms with the concomitant increase of a 6-c LS species. As previously observed for the distal Arg119 and His123 variants (*8*), a negatively charged residue in the distal cavity destabilizes the heme pocket, probably as a consequence of the vicinity of the negatively charged Asp152 residue which is present only in KatGs.

Although the Asn153 residue is not directly located in the active site, it is able to exert an influence through a hydrogen bond with the distal His. Replacing the hydrogen-acceptor carboxamide group by an aspartate carboxylate group or an aliphatic residue alters or breaks this hydrogen bond. As a consequence, the basicity of His123 is altered. It is well-known that the distal His controls ligand binding in heme proteins and it is important in fine-tuning ligand affinities via hydrogen-bond stabilization involving the N_ϵ proton. In peroxidases, it has been proposed (*28*) that the distal His acts as a hydrogen-bond partner in the catalytic cycle, acting as a hydrogen-bond acceptor for the proton from hydrogen peroxide as the latter binds the heme iron. The acid/base catalytic function of the distal His in peroxidases is due to the presence of the positively charged guanidinium group of the distal Arg in the proximity of the His, which in CCP depresses its pK_a to values between 4 and 5 (*29*) and/or to the hydrogen bond between the N_δ proton of the distal His and the Asn. Spectroscopic studies of CCP have provided evidence that the distal His functions as a hydrogen-bond partner to heme-ligated CN (*30*, *31*) and heme-ligated F (*32*). In the latter case, the distal His is hydrogen bonded to a water molecule which is in turn strongly interacting with the fluoride (*33*). The binding constants of fluoride and cyanide were decreased in the CCP variants where the distal Asn was mutated and the His−Asn hydrogen bond was broken or altered (*31*, *32*, *34*). In KatG, the binding of cyanide (*10*) and fluoride also decreases in the corresponding mutants suggesting that the distal Asn−His hydrogen bond renders the distal His basic as in CCP. However, the overall peroxidase activity is similar to WT KatG (*10*), but 1 order of magnitude reduction in catalase activity was observed upon mutation of the Asn153 residue (Table 2). Unfortunately, for CCP the effect of disruption of the His−Asn couple on its peroxidase activity has not been reported. However, data on the corresponding Asn70Val and Asn70Asp variants of HRPC showed that the rates of compound I formation were reduced by about 10% with respect to the native enzyme (*35*−*37*). Moreover, a RR study on these latter variants showed that mutation alters the coordination state giving rise to a 6-c HS heme in both variants, destroys the hydrogen bond between the distal His and the bound CN, and affects the Fe−His bond on the proximal side (*38*). These spectroscopic data are in perfect agreement with the present findings since in both Asn KatG variants a higher amount of a 6-aquo HS heme is found. It appears that the decreased basicity of the distal His, prevents its binding with the distal water molecule which, therefore, binds to the heme iron.

Upon mutation of the distal Asn153 residue selective marked effects on the proximal side are also observed. In common with HRPC, the rupture of the hydrogen bond between Asn153 and His123 in the N153A variant relaxes the protein structure and weakens the hydrogen bond between the proximal His290 and Asp402 residues, whereas the substitution of Asn by Asp does not give rise to any significant change in the proximal side of the heme pocket.

In regard to the Asp152 residue, recent data have shown that the Asp152 variants exhibit a dramatically reduced catalase activity but an increased peroxidase activity indicating that the distal Asp has an essential role in the bifunctional activity of KatGs (Table 2) (*10*). The present data clearly reveal that replacement of the Asp with Ser makes the architecture of the protein very similar to that of CCP. The disappearance of the negative charge in the proximity of the distal cavity results in the rupture of the hydrogen bonds with the two water molecules of the distal cavity which probably leave the cavity. As a consequence, a readjustment of the remaining distal water molecules which form an extended hydrogen-bond network connecting the distal Trp, His, Arg and Asp can be expected. The result is a 5-c HS heme with a vacant sixth coordination position of the heme iron, as in CCP, which also might enhance the peroxidase activity. Moreover, D152 mutation affects the pK_a of the alkaline transition of the reduced protein as well as the Fe−Im bond on the proximal side. Interestingly, in the D152S variant the behavior and the frequencies of the Fe−Im stretches resemble very closely those of CCP, where the two bands at 247 and 233 cm^{-1} arise from two tautomers of the hydrogen-bond between the proximal His and an aspartic

carboxylate side chain (*16*). The RR spectra of the ferrous D152S mutant clearly show that the I_{237}/I_{250} intensity ratio between the two bands increases going from lower to higher pH. Therefore, in analogy to CCP, these two bands are assigned to two tautomers of the hydrogen bond between the His290 and Asp402 carboxylate side chain. In one tautomer (237 cm^{-1}), the proton is closer to the imidazole, while in the other, the proton is almost transferred to the carboxylate group. At alkaline pH, the 237 cm^{-1} increases in intensity at the expense of the 250 cm^{-1} since the hydrogen bond is weakened. The band at 205 cm^{-1}, on the other hand, corresponds to a species whose proton resides on the imidazole as in the native KatG. Its intensity enhancement at alkaline pH (not observed in the WT protein) confirms that the proximal hydrogen bond is weakened. On the contrary, the mutation of the Asp152 to Asn does not alter the proximal Fe−Im bond, the ferrous RR spectrum being almost identical to that of WT. By inspection of the X-ray structure of *Haloarcula marismortui* (*2*), we found that oxygen atom (O1) of the carboxylate groups of the corresponding Asp125 (Asp152 in *Synechocystis* KatG) residue is hydrogen bonded to the nitrogen atom of Ile217 (2.7 Å) (Ile248 in *Synechocystis* KatG), which is part of the KatG-specific insertion LL1 (residues 182−232, *Haloarcula* numbering). This insertion is at one edge of the heme, and connects the distal side with the proximal helices E and F, the latter carrying the proximal His ligand. Since this loop is conserved in KatGs, it is not surprising that alteration of the Asp−Ile hydrogen bond is capable of severely altering the proximal His−Asp interaction. The present results suggest that, unlike the D152S variant, in the D152N variant the Asp−Ile hydrogen bond is not changed and the protein maintains the proximal characteristics of the native protein.

The D152W variant is characterized by three Fe−Im stretches: a very weak band at 237 cm^{-1}, observed mainly at pH 8.5, and two bands that correspond to those observed in the WT protein. It is interesting that the mutation has slightly strengthened the proximal hydrogen bond, because the two latter Fe−Im stretches are at higher frequency than those of WT KatG. The Trp residue is capable of a hydrogen-bond interaction via the nitrogen atom of the indole ring as in WT KatG and the D152N variant; however, the steric hindrance of the indole ring requires readjustments of the architecture of the LL1 loop. A displacement of the loop might give rise to the spectroscopic changes observed on the Fe−Im strength.

Hydrogen-Bond Networks. The present analysis suggests marked differences in the structural role of the conserved residues and hydrogen-bond networks in KatG and CCP which might be connected with their different catalytic activity.

Proximal Side. Why does manipulation of the Trp−Asp interaction in CCP not affect the protein to the same extent as for KatG? The catalytic activity of both proteins depends on the integrity of proximal side residues. In fact, in CCP the Trp191 side chain resides in a K^+ binding site, created by partial negative charges, that envelopes its side chain and is probably necessary to stabilize the Trp191 radical. In CCP, upon mutation of the proximal Trp, cations bind in the cavity created when Trp191 is replaced by Gly or Gln, stabilizing, therefore, the protein architecture. The comparison of the structure of KatGs (*2*, *3*) and CCP (*39*) suggests that the electrostatic environment of KatG is very similar to that of CCP. However, the existence of a porphyrin cation radical has been observed for KatGs (*40*−*43*) and mutation of the proximal Trp does not lead to an alteration of compound I (*12*, *43*). Moreover, recently performed multifrequency EPR spectroscopy in combination with isotopic labeling revealed the formation of tyrosyl and tryptophanyl radicals in *Synechocystis* KatG during reaction of the resting enzyme with peracetic acid and suggested the tryptophan radical to be Trp106, a residue not present in the proximal side (*43*). All these results indicate that the mechanism governing the migration of the radical is different from CCP and that, unlike CCP, the disruption of the Trp−Asp hydrogen bond by mutation destabilizes the protein and weakens the heme binding to the protein, indicating that the proximal residues play a major role in the stability of the protein architecture. Moreover, the different behavior observed for the D402E protein with respect to the D402N variant and WT also suggests that, unlike CCP, in KatG the His−Asp hydrogen bond helps to maintain protein stability. In fact, upon disruption of this hydrogen bond the protein loses the heme, but when the hydrogen bond is partially conserved, as in the case of the D402E variant, the protein maintains some characteristics of KatG.

Distal Side. The His−Asn hydrogen bond maintains the basicity of the distal His, which is important for compound I formation (i.e., hydrogen peroxide reduction) and for the stabilization via hydrogen bond of the external ligands as well as the internal water molecule bound to the heme iron. This role appears to be in common not only with class I peroxidases but with all the plant peroxidases. What is really a peculiar feature of KatG is the presence of a distal Asp residue which is not conserved in plant peroxidases. The present results clearly indicate that in the absence of its carboxylate group hydrogen bonded to two water molecules of the heme distal pocket, the iron atom sixth coordination position becomes almost completely vacant. Moreover, the Asp152 residue represents an important link connecting the proximal and the distal sides of the heme cavity in addition to the conserved hydrogen-bonded networks identified in many plant peroxidases by both crystal structures and spectroscopic techniques (*16*, *44*). This connection involves the distal His123, Asn153, and Asp152 residues and the LL1 loop. The data on the different Asp variants revealed that substitution with Ser makes KatG structurally similar to CCP. Conversely, it is necessary to maintain the hydrogen bond with the Ile residue, as in the case of the Asp/Asn mutation, to keep the Fe−Im bond strength of the WT KatG. These results give a clear indication that the Asp−Ile hydrogen bond is important for the stability of the heme architecture, and for maintaining the proximal hydrogen-bond strength. It is worth noting that Ile217 (Ile248 in *Synechocystis* KatG) is adjacent to Tyr218 (Tyr249 in *Synechocystis* KatG), which is part of the novel KatG specific covalent adduct (that includes also a conserved Met and the distal Trp), and that both residues are part of LL1. However, recent results have shown that while mutation of the Tyr218 residue weakens the heme binding, it does not cause changes to the hydrogen bonds of the proximal side (*45*).

In conclusion, the presented data suggest marked differences in the hydrogen-bond networks in KatG and CCP. Table 2 clearly demonstrates that manipulation of residues

involved in the hydrogen-bond network in KatG mainly affects the catalase but not the peroxidase activity. This suggests, assuming that the initial reaction in both cycles is identical (i.e., compound I formation), that oxidation of the second incoming H_2O_2 molecule (compound I reduction) makes high demands on the protein integrity. From a thermodynamic point of view each peroxidase compound I should be able to oxidize H_2O_2 to molecular oxygen [E'° (O_2/H_2O_2) = 280 mV], nevertheless the catalase activity of peroxidases (exception KatG) can be neglected. But how does a catalase-peroxidase resolve the dilemma of selecting the second small neutral and polar hydrogen peroxide to bind and oxidize it efficiently? Inspection of the structures of monofunctional catalases (*46*) and catalase-peroxidases (*2*, *3*) clearly indicates that (i) the heme is buried deeply inside the protein and the narrow substrate access channel to a maximum of 3−4 Å effectively allows only water, hydrogen peroxide, or other small molecules to reach the heme center; (ii) the presence of a well-defined extensive hydrogen-bond network selectively guides the binding of the second peroxide molecule. It has been shown for monofunctional catalases that variants that widen the substrate channel possess lower catalase activity (*46*). Although in these studies no distinction was made between the H_2O_2 reduction and oxidation reaction, it is reasonable to assume that also in monofunctional catalases disruption of the ordered hydrogen-bond network at the distal side strongly influences the oxidation of H_2O_2 but not its reduction. Further experiments, including resonance Raman spectroscopy of compound I of recombinant KatG and selected mutants, are necessary to understand the catalase activity of these enzymes.

REFERENCES

1. Welinder, K. G. (1992) Superfamily of plant, fungal and bacterial peroxidases. *Curr. Opin. Struct. Biol. 2*, 388−393.
2. Yamada, Y., Fujiwara, T., Sato, T., Igarashi, N., and Tanaka, N. (2002) The 2.0 Å crystal structure of catalase-peroxidase from *Aloarcula marismortui*. *Nat. Struct. Biol. 9*, 691−695.
3. Carpena, X., Loprasert, S., Mongkolsuk, S., Switala, J., Loewen, P. C., and Fita, I. (2003) Catalase-peroxidase KatG of *Burkholderia pseudomallei* at 1.7 Å resolution. *J. Mol. Biol. 327*, 475−489.
4. Donald, L. J., Krokhin, O. V., Duckworth, H. W., Wiseman, B., Deemagarn, T., Singh, R., Switala, J., Carpena, X., Fita, I., and Loewen, P. C. (2003) Characterization of the catalase-peroxidase KatG from *Burkholderia pseudomallei* by mass spectroscopy. *J. Biol. Chem. 278*, 35687−35692.
5. Jakopitsch, C., Kolarich, D., Petutschnig, G., Furtmüller, P. G., and Obinger, C. (2003) Distal side tryptophan, tyrosine and methionine in catalase-peroxidases are covalently linked in solution. *FEBS Lett. 552*, 135−140.
6. Regelsberger, G., Jakopitsch, C., Rükers, F., Krois, D., Peschek, G. A., and Obinger, C. (2000) Effect of distal cavity mutations on the formation of compound I in catalase-peroxidase. *J. Biol. Chem. 275*, 22854−22861.
7. Regelsberger, G., Jakopitsch, C., Furtmüller, P. G., Rüker, F., Switala, J., Loewen, P. C., and Obinger, C. (2001) The role of distal tryptophan in the bifunctional activity of catalase-peroxidase. *Biochem. Soc. Trans. 29*, 99−105.
8. Heering, H. A., Indiani, C., Regelsberger, G., Jakopitsch, C., Obinger, C., and Smulevich, G. (2002) New insights into the heme cavity structure of catalase-peroxidase: a spectroscopic approach to the recombinant *Synechocystis* enzyme and selected distal cavity mutants. *Biochemistry 41*, 9237−9247.
9. Jakopitsch, C., Regelsberger, G., Furtmüller, P. G., Rüker, F., Pescheck, G. A., and Obinger, C. (2002) Engineering the proximal heme cavity of catalase-peroxidase. *J. Inorg. Biochem. 91*, 78−86.
10. Jakopitsch, C., Auer, M., Regelsberger, G., Jantschko, W., Furtmüller, P. G., Rüker, F., and Obinger, C. (2003) Distal site aspartate is essential in the catalase activity of catalase-peroxidase. *Biochemistry 42*, 5292−5300.
11. Jakopitsch, C., Auer, M., Regelsberger, G., Jantschko, W., Furtmüller, P. G., Rüker, F., and Obinger, C. (2003) The catalytic role of the distal site asparagine-histidine couple in catalase-peroxidase. *Eur. J. Biochem. 270*, 1006−1013.
12. Yu, S., Chouchane, S., and Magliozzo, R. S. (2002) Characterization of the W321F mutant of *Mycobacterium tubercolosis* catalase-peroxidase KatG. *Protein Sci. 11*, 58−64.
13. Marzocchi, M. P., and Smulevich, G. (2003) Relationship between heme vinyl conformation and the protein matrix in peroxidases. *J. Raman Spectrosc. 34*, 725−736.
14. Kalsbeck, W. A., Ghosh, A., Pandey, R. K., Smith, K. M., and Bocian, D. F. (1995) Determinants of the vinyl stretching frequency in protoporphyrins. Implications for cofactor-protein interactions in heme proteins. *J. Am. Chem. Soc. 117*, 10959−10968.
15. Smulevich, G., Hu, S. Z., Rodgers, K. R., Goodin, D. B., Smith, K. M., and Spiro, T. G. (1996) Heme-protein interactions in cytochrome *c* peroxidase revealed by site-directed mutagenesis and resonance Raman spectra of isotopically labeled hemes. *Biospectroscopy 2*, 365−376.
16. Smulevich, G., Mauro, J. M., Fishel, L. A., English, A., Kraut, J., and Spiro, T. G. (1988) Heme pocket interactions in cytochrome *c* peroxidase studied by site-directed mutagenesis and resonance Raman spectroscopy. *Biochemistry 27*, 5477−5485.
17. Smulevich, G. (1998) Understanding the heme cavity structure of peroxidases: comparison of electronic absorption and resonance Raman spectra with crystallographic results. *Biospectroscopy 4*, S3−S17.
18. Goodin, D. B., and McRee, D. E. (1993) The Asp-His-Fe triad of cytochrome *c* peroxidase controls the reduction potential, electronic structure, and coupling of the tryptophan free radical to the heme. *Biochemistry 32*, 3313−3324.
19. Miller, M. A., Shaw, A., and Kraut, J. (1994) 2.2 Å structure of oxy-peroxidase as a model for the transient enzyme: peroxidase complex. *Nat. Struct. Biol. 1*, 524−531.
20. Sundaramoorthy, M., Choudhury, K., Edwards, M., and Poulos, T. L. (1991) Crystal structure and Preliminary functional analysis of the cytochrome *c* peroxidase His175Gln proximal ligand mutant. *J. Am. Chem. Soc. 113*, 7755−7757.
21. Wang, J., Mauro, J. M., Edwards, S. L., Oatley, S. J., Fishel, L. A., Ashford, V. A., Xuong, N., and Kraut, J. (1990) X-ray structures of recombinant yeast cytochrome *c* peroxidase and three heme-cleft mutants prepared by site-directed mutagenesis. *Biochemistry 29*, 7160−7173.
22. Mauro, J. M., Fishel, L. A., Hazzard, J. T., Meyer, T. E., Tollin, G., Cusanovich, M. A., and Kraut, J. (1988) Tryptophan191 → phenylalanine, a proximal side mutation in yeast cytochrome *c* peroxidase that strongly affects the kinetics of ferrocytochrome *c* oxidation. *Biochemistry 27*, 6243−6256.
23. Sivaraja, M., Goodin, D. B., Smith, M., and Hoffman, B. M. (1989) Identification by endor of Trp191 as the free-radical site in cytochrome *c* peroxidase in compound ES. *Science 245*, 738−740.
24. Patterson, W. R., and Poulos, T. L. (1995) Crystal structure of recombinant pea cytosolic ascorbate peroxidase. *Biochemistry 34*, 4331−4341.
25. Pappa, H. S., Patterson, W. R., and Poulos, T. L. (1996) The homologous tryptophan critical for cytochrome *c* peroxidase function is not essential for ascorbate peroxidase activity. *J. Biol. Inorg. Chem. 1*, 61−66.
26. Marquez, L. A., Quitoriano, M., Zilinskas, B. A., and Dunford, H. B. (1996) Kinetic and spectral properties of pea cytosolic ascorbate peroxidase. *FEBS Lett. 389*, 153−156.
27. Howes, B. D., Veitch, N. C., Smith, A. T., White, C. G., and Smulevich, G. (2001) Haem-linked interactions in horseradish peroxidase revealed by spectroscopic analysis of the Phe-221 → Met mutant. *Biochem. J. 353*, 181−191.
28. Poulos, T. L. and Kraut, J. (1980) The stereochemistry of peroxidase catalysis. *J. Biol. Chem. 255*, 8199−8205.
29. Smulevich, G., Miller, M. A., Kraut, J., and Spiro, T. G. (1991) Conformational Change and Histidine Control of Heme Chemistry in Cytochrome-*c* Peroxidase − Resonance Raman Evidence from Leu-52 and Gly-181 Mutants of Cytochrome-*c* Peroxidase. *Biochemistry 30*, 9546−9558.

30. Satterlee, J. D., and Erman, J. E. (1991) Proton NMR assignment of heme contacts and catalytically implicated amino acids in cyanide-ligated cytochrome *c* peroxidase determined from one- and two- dimensional nuclear Overhauser effects. *Biochemistry 30*, 4398−4405.
31. Satterlee, J. D., Alam, S. L., Mauro, J. M., Erman, J. E., and Poulos, T. L. (1994) The effect of the Asn82→Asp mutation in yeast cytochrome *c* peroxidase studied by proton NMR spectroscopy. *Eur. J. Biochem. 224*, 81−87.
32. DeLauder, S. F., Mauro, J. M., Poulos, T. L., Williams, J. C., and Schwartz, F. P. (1994) Thermodynamics of hydrogen cyanide and hydrogen fluoride binding to cytochrome *c* peroxidase and its Asn82Asp mutant. *Biochem. J. 302*, 437−442.
33. Edwards, S. L. and Poulos, T. L. (1990) Ligand binding and structural perturbations in cytochrome *c* peroxidase. *J. Biol. Chem. 265*, 2588−2595.
34. Alam, S. L., Satterlee, J. D., Mauro, J. M., Poulos, T. L., and Erman, J. E. (1995) Proton NMR studies of cytochrome *c* peroxidase mutant N82A: hyperfine resonance assignments, identification of two interconverting enzyme species, quantitating the rate of interconversion, and determination of equilibrium constants. *Biochemistry 34*, 15496−15503.
35. Nagano, S., Tanaka, M., Watanabe, Y., and Morishima, I. (1995) Putative hydrogen bond network in the heme distal site of horseradish peroxidase. *Biochem. Biophys. Res. Commun. 207*, 417−423.
36. Nagano, S., Tanaka, M., Ishimori, K., Watanabe, Y., and Morishima, I. (1996) Catalytic roles of the distal site asparagine-histidine couple in peroxidases. *Biochemistry 35*, 14251−14258.
37. Tanaka, M., Nagano, S., Ishimori, K., and Morishima, I. (1997) Hydrogen bond network in the distal site of peroxidases: spectroscopic properties of Asn → Asp horseradish peroxidase mutant. *Biochemistry 36*, 9791−9798.
38. Mukai, M., Nagano, S., Tanaka, M., Ishimori, K., Morishima, I., Ogura, T., Watanabe, Y., and Kitagawa, T. (1997) Effects of concerted hydrogen bonding of distal histidine on active site structures of horseradish peroxidase. Resonance Raman studies with Asn70 mutants. *J. Am. Chem. Soc. 119*, 1758−1766.
39. Finzel, B. C., Poulos, T. L., and Kraut, J. (1984) Crystal structure of yeast cytochrome *c* peroxidase refined at 1.7 Å resolution. *J. Biol. Chem. 259*, 13027−13036.
40. Hillar, A., Peters, B., Pauls, R., Loboda, A., Zhang, H., Mauk, A. G., and Loewen, P. C. (2000) Modulation of the activities of catalase-peroxidase HPI of *Escherichia coli* by site-directed mutagenesis. *Biochemistry 39*, 5868−5875.
41. Chouchane, S., Girotto, S., Shengwei, Y., and Magliozzo, R. S. (2002) Identification and characterization of tyrosyl radical formation in *Mycobacterium tubercolosis* catalase-peroxidase (KatG). *J. Biol. Chem. 277*, 42633−42638.
42. Jakopitsch, C., Auer, M., Ivancich, A., Rüker, F., Furtmüller, P. G., and Obinger, C. (2003) Total conversion of bifunctional catalase-peroxidase (KatG) to monofunctional peroxidase by exchange of a conserved distal side tyrosine. *J. Biol. Chem. 278*, 20185−20191.
43. Ivancich, A., Jakopitsch, C., Auer, M., Un, S., and Obinger, C. (2003) Protein-based radicals in the catalase-peroxidase of *Synechocystis* PCC6803: a multifrequency EPR investigation of wild-type and variants on the environment of the heme active site. *J. Am. Chem. Soc. 125*, 14093−14102.
44. Dunford, H. B. (2001) How do enzymes work? Effect of electron circuits on transition state acid dissociation constants. *J. Biol. Inorg. Chem. 6*, 819−822.
45. Santoni, E., Jakopitsch, C., Obinger, C., and Smulevich, G. (2004) Manipulating the covalent link between distal side tryptophan, tyrosine and methionine in catalase-peroxidase: an electronic absorption and resonance Raman study. *Biopolymers*, in press.
46. Nicholls, P., Fita, I., and Loewen, P. C. (2001) Enzymology and structure of catalases, *Adv. Inorg. Chem.* 51, 51−106.

BI035835B